Monthly Notices
of the
ROYAL ASTRONOMICAL SOCIETY

MNRAS **458,** 3134–3149 (2016)
Advance Access publication 2016 February 22

doi:10.1093/mnras/stw409

ALMA observations of cold molecular gas filaments trailing rising radio bubbles in PKS 0745−191

H. R. Russell,[1⋆] B. R. McNamara,[2,3] A. C. Fabian,[1] P. E. J. Nulsen,[4,5] A. C. Edge,[6] F. Combes,[7] N. W. Murray,[8] I. J. Parrish,[8] P. Salomé,[7] J. S. Sanders,[9] S. A. Baum,[10] M. Donahue,[11] R. A. Main,[8] R. W. O'Connell,[12] C. P. O'Dea,[10] J. B. R. Oonk,[13,14] G. Tremblay,[15] A. N. Vantyghem[2] and G. M. Voit[11]

[1]*Institute of Astronomy, Madingley Road, Cambridge CB3 0HA, UK*
[2]*Department of Physics and Astronomy, University of Waterloo, Waterloo, ON N2L 3G1, Canada*
[3]*Perimeter Institute for Theoretical Physics, Waterloo, ON N2L 2Y5, Canada*
[4]*Harvard–Smithsonian Center for Astrophysics, 60 Garden Street, Cambridge, MA 02138, USA*
[5]*ICRAR, University of Western Australia, 35 Stirling Hwy, Crawley, WA 6009, Australia*
[6]*Department of Physics, Durham University, Durham DH1 3LE, UK*
[7]*Observatoire de Paris, LERMA, 61 Av. de l'Observatoire, F-75014 Paris, France*
[8]*Canadian Institute for Theoretical Astrophysics, University of Toronto, 60 St. George Street, Toronto, M5S 3H8 ON, Canada*
[9]*Max-Planck-Institut für extraterrestrische Physik, Giessenbachstrasse 1, D-85748 Garching, Germany*
[10]*University of Manitoba, Department of Physics and Astronomy, Winnipeg, MB R3T 2N2, Canada*
[11]*Department of Physics and Astronomy, Michigan State University, 567 Wilson Road, East Lansing, MI 48824, USA*
[12]*Department of Astronomy, University of Virginia, PO Box 400235, Charlottesville, VA 22904, USA*
[13]*Netherlands Institute for Radio Astronomy (ASTRON), Postbus 2, NL-7990 AA Dwingeloo, the Netherlands*
[14]*Leiden Observatory, Leiden University, PO Box 9513, NL-2300 RA Leiden, the Netherlands*
[15]*Department of Physics and Yale Center for Astronomy and Astrophysics, Yale University, 217 Prospect Street, New Haven, CT 06511, USA*

Accepted 2016 February 18. Received 2016 February 17; in original form 2016 January 18

ABSTRACT

We present ALMA observations of the CO(1–0) and CO(3–2) line emission tracing filaments of cold molecular gas in the central galaxy of the cluster PKS 0745−191. The total molecular gas mass of $4.6 \pm 0.3 \times 10^9$ M$_\odot$, assuming a Galactic $X_{\rm CO}$ factor, is divided roughly equally between three filaments each extending radially 3−5 kpc from the galaxy centre. The emission peak is located in the SE filament ∼1 arcsec (2 kpc) from the nucleus. The velocities of the molecular clouds in the filaments are low, lying within ±100 km s^{-1} of the galaxy's systemic velocity. Their full width at half-maximum (FWHM) are less than 150 km s^{-1}, which is significantly below the stellar velocity dispersion. Although the molecular mass of each filament is comparable to a rich spiral galaxy, such low velocities show that the filaments are transient and the clouds would disperse on $<10^7$ yr time-scales unless supported, likely by the indirect effect of magnetic fields. The velocity structure is inconsistent with a merger origin or gravitational free-fall of cooling gas in this massive central galaxy. If the molecular clouds originated in gas cooling even a few kpc from their current locations their velocities would exceed those observed. Instead, the projection of the N and SE filaments underneath X-ray cavities suggests they formed in the updraft behind bubbles buoyantly rising through the cluster atmosphere. Direct uplift of the dense gas by the radio bubbles appears to require an implausibly high coupling efficiency. The filaments are coincident with low temperature X-ray gas, bright optical line emission and dust lanes indicating that the molecular gas could have formed from lifted warmer gas that cooled *in situ*.

Key words: galaxies: active – galaxies: clusters: individual: PKS 0745−191 – galaxies: evolution.

1 INTRODUCTION

The cores of rich galaxy clusters host the brightest and most massive galaxies known. These brightest cluster galaxies (BCGs) are

⋆ E-mail: hrr27@ast.cam.ac.uk

giant ellipticals with extended, diffuse stellar envelopes and predominantly old, 'red and dead' stellar populations. However, not all BCGs are passively evolving at late times. Those residing beneath cooling hot atmospheres commonly feature luminous, filamentary emission line nebulae, cold molecular gas reservoirs with masses above 10^9 M$_\odot$ to a few $\times 10^{10}$ M$_\odot$ and star formation rates at several to tens of solar masses per year (Heckman 1981; Hu, Cowie & Wang 1985; Johnstone, Fabian & Nulsen 1987; McNamara & O'Connell 1992; Jaffe & Bremer 1997; Edge 2001; Salomé & Combes 2003). Cool core galaxy clusters have hot X-ray atmospheres with short central radiative cooling times, which can drop below a gigayear. An unimpeded flow of gas cooling from the cluster atmosphere would be expected to supply at least an order of magnitude more cold gas and star formation than is observed in BCGs in cool core clusters (Fabian 1994; Peterson & Fabian 2006). Instead, high-resolution X-ray images from *Chandra* show that powerful radio jets, launched by the central radio AGN, are inflating large, buoyant radio bubbles and generating shocks, sound waves and turbulence which heat the cluster atmosphere and suppress gas cooling (e.g. McNamara & Nulsen 2007, 2012; Fabian 2012). The energy input by the AGN is sufficient to replace the X-ray radiative losses for large samples of groups and clusters and appears to be closely coupled to the cooling rate in a feedback loop (Bîrzan et al. 2004; Dunn & Fabian 2006; Rafferty et al. 2006). This mechanism is likely operating to suppress gas cooling and star formation in all massive elliptical galaxies at late times (Bower et al. 2006; Croton et al. 2006; Best et al. 2007).

This radio-mode (mechanical) feedback prevents the bulk of the volume-filling hot atmospheres in galaxies and clusters from cooling to low temperatures, but whether it can also regulate the supply of dense, cold molecular gas is not known. Cold gas and recent star formation in BCGs are likely fuelled by gas cooling from the cluster atmosphere, albeit at rates well below the expectations of cooling flows. Correlations between the X-ray cooling rate and star formation rates (Egami et al. 2006; O'Dea et al. 2008) and the detection of star formation and luminous emission line nebulae predominantly in systems with central cooling times below a sharp threshold at $\sim 5 \times 10^8$ yr support this picture (Cavagnolo et al. 2008; Rafferty, McNamara & Nulsen 2008). Accretion of this cold gas is likely a key element of feedback linking the gas cooling rate to the fuelling of the SMBH and the energy output of the AGN (e.g. Pizzolato & Soker 2005; Gaspari, Brighenti & Temi 2015). Radio-jet driven outflows of ionized and molecular gas have been detected in nearby radio galaxies suggesting that jets can couple to dense gas clouds (Morganti, Tadhunter & Oosterloo 2005; Nesvadba et al. 2006; Alatalo et al. 2011; Dasyra & Combes 2011; Morganti et al. 2015). In NGC 1275 at the centre of the Perseus cluster, the velocity structure of extended H α filaments, which are coincident with single dish detections of molecular gas, is consistent with uplift under the buoyantly rising radio bubbles (Hatch et al. 2006; Salomé et al. 2006, 2011). Inflowing molecular gas filaments are also observed closer to the galaxy centre (Lim, Ao & Dinh-V-Trung 2008). ALMA Early Science observations of Abell 1835 showed a much more substantial uplift with 10^{10} M$_\odot$ of molecular gas in a high-velocity flow underneath the buoyant radio bubbles (McNamara et al. 2014).

Here, we present ALMA Cycle 1 observations of the molecular gas in the PKS 0745−191 BCG, which with $P_{\rm cav} \sim 5 \times 10^{45}$ erg s^{-1} has undergone an even more powerful radio jet outburst than Abell 1835 (Rafferty et al. 2006; Sanders et al. 2014). Single dish observations of PKS 0745−191 detected the BCG at CO(1–0) and CO(2–1) and found a total molecular gas mass of $3.8 \pm 0.9 \times 10^9$ M$_\odot$ (Salomé & Combes 2003). Optical, UV and IR observations show significant star formation at a rate of $\sim$20 M$_\odot$ yr^{-1} and a luminous emission line nebula with clumpy filaments extending $>$ 10 kpc in the BCG (Fabian et al. 1985; Johnstone et al. 1987; Donahue et al. 2000; Hicks & Mushotzky 2005; Tremblay et al. 2015). The surrounding rich cluster has a short central cooling time $<5 \times 10^8$ yr and X-ray spectra are consistent with several hundred solar masses per year cooling down below X-ray temperatures. The coolest X-ray gas is offset by $\sim$2.5 arcsec ($\sim$5 kpc) to the W of the hard X-ray and radio point source emission from the low-luminosity AGN, which may be due to sloshing of the hot gas in the cluster potential (Sanders et al. 2014). The ALMA observations now resolve the spatial and velocity structure of the cold molecular gas structures at the centre of the BCG revealing extended filaments trailing the two buoyant radio bubbles.

For a standard ΛCDM cosmology with $H_0 = 70$ km s^{-1} Mpc^{-1}, at the central galaxy's redshift ($z = 0.1028$; Hunstead, Murdoch & Shobbrook 1978) 1 arcsec corresponds to 1.9 kpc. The BCG redshift was determined from optical emission lines, including H α, H β and [O III], which likely originate from the ionized surfaces of the molecular gas clouds making up the extended cool gas nebula (e.g. Jaffe, Bremer & Baker 2005; Hatch et al. 2006; Oonk et al. 2010; Salomé et al. 2011). Bulk motion of the emission line nebula could therefore produce a systematic offset in the gas velocities with respect to the gravitational potential of the BCG. In the absence of stellar absorption line measurements directly tracing the BCG potential, we note that our conclusions on the velocity structure of the molecular gas depend on the redshift from the emission line gas.

2 DATA REDUCTION

The BCG at the centre of PKS 0745−191 was observed by ALMA in Cycle 1 with single pointings to cover the CO(1–0) line at 104.53 GHz in band 3 and the CO(3–2) line at 313.56 GHz in band 7 (ID = 2012.1.00837.S; PI McNamara). The observations were centred on the nucleus of PKS 0745−191 (RA 07:47:31.32, Dec. −19:17:39.97, J2000) and the HPBW of the primary beam was 60 arcsec in band 3 and 20 arcsec in band 7. The data were taken in two 8 min observations in band 3 on 2014 April 26 and 27 and in a 25 min observation in band 7 on 2014 August 19. The observations utilized 32–36 antennas with baselines of 20-560 m at CO(1–0) and a more extended configuration with baselines of 34–1100 m at CO(3–2). The frequency division correlator mode was used with a 1.875 GHz bandwidth and frequency resolution of 488.3 kHz (1.40–0.47 km s^{-1}) but channels were binned together to improve the signal-to-noise ratio. An additional baseband was positioned to image the continuum in each observation.

The observations were calibrated in CASA version 4.2.2 (McMullin et al. 2007) using the ALMA pipeline reduction scripts and additional self-calibration significantly improved the image quality. The continuum-subtracted images were reconstructed using CLEAN and various Briggs weightings were explored to determine the optimum for imaging in each band. A robustness parameter of 0.5 was used for the CO(1–0) cube and a value of 2 was used to maximize the signal to noise in the CO(3–2) cube. This provided a synthesized beam of 1.6 arcsec × 1.2 arcsec with a position angle (P.A.) of 79.°7 at CO(1–0) and 0.27 arcsec × 0.19 arcsec with a P.A. of 78.°3 at CO(3–2). The rms noise in the line-free channels was 0.6 mJy at CO(1–0) and 1 mJy at CO(3–2) for 10 km s^{-1} channels. Images of the continuum emission were also produced by averaging channels free of any line emission. An unresolved central continuum source is detected in both bands with flux 9.30 ± 0.04 mJy at 103.8 GHz and 4.6 ± 0.2 mJy at 314.8 GHz. The position of the

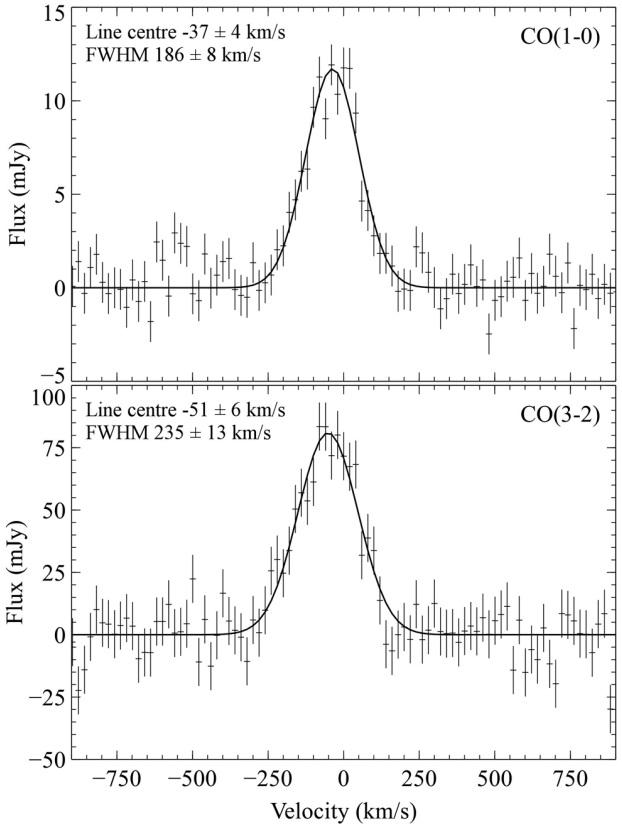

Figure 1. PKS 0745−191 CO(1–0) (top) and CO(3–2) (bottom) total spectra for 6 arcsec × 6 arcsec and 4 arcsec × 4 arcsec regions, respectively. The best-fitting model parameters are given in Table 1.

mm-continuum source coincides with the unresolved radio nucleus detected at 8.64 GHz with the ATCA in 6A configuration (Hogan et al. 2015). The mm-continuum flux is also consistent with the upper limit on synchrotron emission from a flat spectrum radio core[1] with $\alpha = 0.2$ (Hogan et al. 2015) and this is likely to be the location of the low-luminosity AGN.

3 RESULTS

3.1 Gas distribution in the central galaxy

The CO(1–0) and CO(3–2) rotational transition lines were both detected and imaged at the centre of the BCG in PKS 0745−191. The continuum-subtracted total spectral line profiles were extracted from a 6 arcsec × 6 arcsec region for CO(1–0) and a 4 arcsec × 4 arcsec region for CO(3–2) and are shown in Fig. 1. Larger regions produce consistent total fluxes but significantly noisier spectra. Each spectrum was fitted with a single Gaussian component using the package MPFIT (Markwardt 2009) and the best-fitting results, corrected for primary beam response and instrumental broadening, are shown in Table 1. The CO(1–0) and CO(3–2) total spectra are consistent with single velocity components blueshifted from −30 to −50 km s^{-1} and have a comparable full width at half-maximum (FWHM) of 200–230 km s^{-1}. The total CO(1–0) integrated intensity of 2.5 ± 0.2 Jy km s^{-1} is roughly consistent with the IRAM 30 m single dish signal of 1.8 ± 0.4 Jy km s^{-1} (Salomé & Combes 2003) given the significant uncertainties in the continuum baseline subtraction for the earlier detection. This shows that little extended emission has been filtered out by the interferometer at CO(1–0).

Integrated intensity maps of the CO(1–0) and CO(3–2) emission are shown in Fig. 2. The CO(1–0) line emission extends over ∼6 arcsec (11 kpc) with roughly a third of the emission lying within an unresolved central peak that is marginally offset to the SE of the nuclear continuum emission. The CO(1–0) emission extends to the N, SE and SW of the nucleus with a similar morphology to the brightest regions of H α, Pa α and ro-vibrational H_2 (Donahue et al. 2000; Wilman, Edge & Swinbank 2009). The CO(3–2) line emission resolves this extended structure into three filaments each 1.5–2.5 arcsec (3−5 kpc) in length. The SE, SW and N filaments contain roughly 35, 30 and 25 per cent of the total line flux in CO(3–2), respectively. The N filament extends furthest and appears to bend along its length and may be fragmenting at large radius. The peak in the CO(3–2) emission lies 1.1 arcsec to the SE of the nuclear continuum emission. Emission from the SW filament appears to extend across the nucleus and this structure may also include the base of the N filament. However, several structures are likely superimposed at this junction between the three filaments. The molecular gas is clearly not centred on the nucleus and it is difficult to constrain the physical location of the structure along the line of sight.

3.2 Line ratio

The CO(3–2)/CO(1–0) line ratio was calculated for each of the three filaments and a region centred on the nucleus. The CO(3–2) data set was convolved with a 2D Gaussian to match the CO(1–0) synthesized beam and the integrated intensities (in K km s^{-1}) were determined from spectral fitting to each data set using matching CO(1–0) beam-sized regions. The line ratios for the BCG centre, N and SE filaments were consistent within the error with CO(3–2)/CO(1–0) = 0.81 ± 0.05, 0.8 ± 0.1 and 0.9 ± 0.1, respectively. The line ratio measured for the SW filament was significantly lower at CO(3–2)/CO(1–0) = 0.53 ± 0.07. The FWHM measured in each of the four regions is consistent within the errors for both the CO(1–0) and the matched resolution CO(3–2) observation. Assuming that the CO emission is optically thick and the gas is thermalized, the line ratios indicate an excitation temperature of 20–30 K. The gas is therefore highly excited and dense. The lower line ratio for the SW filament is likely due to a lower average molecular density in this region and more diffuse gas.

3.3 Velocity structure

We mapped the velocity structure of the molecular gas by extracting spectra for synthesized beam-sized regions centred on each spatial pixel in the cube. These spectra were fitted with one or two Gaussian components using MPFIT and we required at least 3σ significance for the detection of a line determined using Monte Carlo simulations. As discussed in Section 1, the BCG's systemic velocity has been determined from optical emission line spectra and may therefore be affected by the bulk motion of the emission line gas with respect to the BCG potential. However, the radial distribution of the filaments in PKS 0745−191 appears very different from the one-sided bulk offsets of the emission line gas from the BCG centre in systems undergoing mergers or gas sloshing (Hamer et al. 2012). We therefore do not expect a large velocity offset > 100 km s^{-1} between the gas structures and the stellar potential.

[1] For the convention $f_\nu \propto \nu^{-\alpha}$.

Table 1. Fit parameters for the CO(1–0) and CO(3–2) spectra from different regions.

CO line	ν_{rest} (GHz)	ν_{obs} (GHz)	Region	χ^2/dof	Integrated intensity (Jy km s^{-1})	Peak (mJy)	FWHM (km s^{-1})	Velocity shift (km s^{-1})	Mass[a] (10^9 M$_\odot$)
J=1–0	115.27	104.53	Total	1079/1061	2.2 ± 0.1	10.9 ± 0.4	186 ± 8	−37 ± 4	4.6 ± 0.3
			SE	1072/1058	0.49 ± 0.04	2.4 ± 0.1	190 ± 10	−29 ± 5	
					0.06 ± 0.02	1.0 ± 0.2	50 ± 10	−212 ± 5	
			N	1077/1058	0.43 ± 0.04	2.5 ± 0.1	160 ± 10	−87 ± 6	
					0.04 ± 0.02	1.0 ± 0.3	40 ± 20	28 ± 6	
			SW	1070/1061	0.45 ± 0.04	2.7 ± 0.1	160 ± 10	−27 ± 4	
J=3–2	345.80	313.56	Total	350/357	18.6 ± 1.4	74 ± 4	235 ± 13	−51 ± 6	
			Nuc.	332/354	0.7 ± 0.2	1.8 ± 0.4	390 ± 70	−130 ± 30	
					0.26 ± 0.09	2.9 ± 0.6	80 ± 20	−68 ± 8	
			SW1	374/357	0.97 ± 0.07	8.0 ± 0.4	114 ± 6	−6 ± 3	
			SW2	340/354	0.58 ± 0.08	7.3 ± 0.5	75 ± 9	−39 ± 4	
					0.17 ± 0.09	1.9 ± 0.5	90 ± 40	60 ± 20	
			SE1	371/357	1.62 ± 0.09	7.1 ± 0.3	214 ± 9	−24 ± 4	
			SE2	351/354	1.8 ± 0.4	5 ± 1	310 ± 30	−10 ± 10	
					0.8 ± 0.2	6 ± 1	130 ± 20	−49 ± 5	
			N1	401/357	0.53 ± 0.08	3.7 ± 0.4	130 ± 20	−142 ± 6	
			N2	372/354	0.37 ± 0.07	3.1 ± 0.4	110 ± 20	−161 ± 7	
					0.18 ± 0.05	2.9 ± 0.5	60 ± 10	3 ± 5	
			N3	382/354	0.34 ± 0.07	4.3 ± 0.6	80 ± 10	−151 ± 6	
					0.2 ± 0.1	1.8 ± 0.4	130 ± 50	−30 ± 20	
			N4	371/357	0.37 ± 0.06	4.6 ± 0.4	77 ± 9	−145 ± 4	
			N5	346/357	0.28 ± 0.06	3.6 ± 0.5	70 ± 10	−69 ± 5	

Note. [a]The molecular gas mass was calculated from the CO(1–0) integrated intensity as described in Section 3.5.

Figs 3 and 4 show the line centre and FWHM for each of the detected velocity components at CO(1–0) and CO(3–2), respectively. The gas velocities lie within ±100 km s^{-1} of the systemic velocity. Furthermore, the FWHM lies below 200 km s^{-1} across most of the extended structure. At CO(1–0), the gas velocity centre ranges from -87 ± 6 km s^{-1} north of the nucleus to -50 ± 10 km s^{-1} in the SE and -27 ± 4 km s^{-1} in the SW. Additional velocity components are detected to the N and SE of the nucleus. These additional velocity components appear narrower than the main component with FWHM of 40 ± 20 and 50 ± 10 km s^{-1} to the N and SE, respectively. Fig. 5 shows regions selected to cover these detections of multiple velocity components and Figs 6 and 7 show the spectra extracted from these regions and the best-fitting models. Fig. 6 shows the best-fitting models for the multiple velocity components detected in the N and SE regions and for the SW region where a second component is not significantly detected. The second velocity component is redshifted to 28 ± 6 km s^{-1} to the N and blueshifted to -212 ± 5 km s^{-1} to the SE. In each case, the flux of the additional component is roughly 10 per cent of the primary velocity component.

The velocity structure at CO(3–2) is clearly resolved into three main filaments but appears broadly similar to the CO(1–0) structure. The N filament contains predominantly blueshifted gas with velocity centres from -161 ± 7 to -142 ± 6 km s^{-1} and this decreases to -49 ± 5 and -39 ± 4 km s^{-1} in the SE and SW filaments, respectively. The FWHM is less than 150 km s^{-1} along the N and SW filaments except for a region of redshifted emission to the NW where the FWHM increases to 260 ± 30 km s^{-1}. The N filament appears to bend to the NW at its furthest extent and may be breaking up in this region. Additional velocity components are clearly detected in the N and SE filaments, roughly coincident with the additional velocity components detected at CO(1–0). This second component has a velocity centre of -30 ± 20 km s^{-1} to 3 ± 5 km s^{-1} in the N filament and −49 km s^{-1} in the SE filament. The FWHM is greatest at 200–300 km s^{-1} for the majority of the gas in the SE filament. The additional velocity components appear broader at CO(3–2) with FWHM of 60–130 km s^{-1} in the N filament and 130 ± 20 km s^{-1} in the SE filament. At CO(3–2), a second velocity component is also detected at a radius of 1.6 arcsec (3 kpc) along the SW filament and a broad component with FWHM of 390 ± 70 km s^{-1} is coincident with the nucleus (Figs 4 and 7). The fraction of the flux in the second velocity component compared to the total emission in each filament is ∼10 per cent, which is similar to the fraction at CO(1–0).

In summary, the velocities of the molecular gas are low, lying within ±100 km s^{-1} of the galaxy's systemic velocity. The FWHM lies below 200 km s^{-1} across most of the extended structure, which is significantly below the stellar velocity dispersion of BCGs (e.g. von der Linden et al. 2007). The velocity structure is therefore inconsistent with gravitational motions within the galaxy.

3.4 Velocity profiles

Fig. 4 shows ordered velocities along the N and SW filaments. We have produced position–velocity (PV) cuts along each of the filaments resolved in the higher spatial resolution CO(3–2) observations to identify velocity gradients (Fig. 8). Fig. 8 (upper left) shows the axis used for each PV slice, which summed the line emission across the width of each filament (0.2−0.3 arcsec). The N filament has a shallow velocity gradient from −150 to 50 km s^{-1} over 2.5 arcsec (4.8 kpc). The inner region of this filament shows the two velocity components detected within 1 arcsec of the nucleus at −150 km s^{-1} and at the BCG's systemic velocity. The SE filament contains the broadest velocity component with an FWHM of 300 km s^{-1}. The gas clouds in this filament could be moving nearly along the line of sight and therefore at a different orientation the velocity structure would be similar to the other two filaments. The two intensity peaks in the SE filament have similarly broad FWHM and they may be physically separate along the line of sight.

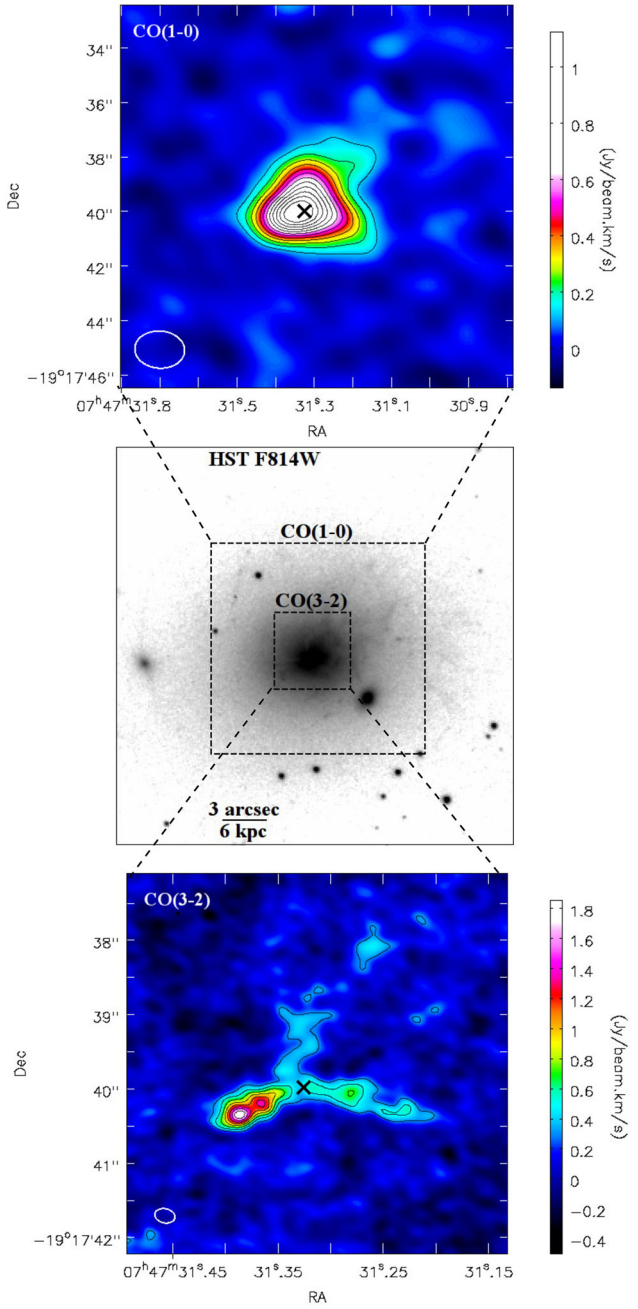

Figure 2. Top: CO(1–0) integrated intensity map for velocities −240 to 160 km s^{-1}. Centre: *HST F814W* image of the BCG at the centre of PKS 0745−191 with regions corresponding to the size of the ALMA images overlaid. The image includes the H α+[N II] line emission and the old stellar population with a half-light radius of ∼20 kpc (2MASS extended source *K* band; Skrutskie et al. 2006). Bottom: CO(3–2) integrated intensity map for velocities −240 to 180 km s^{-1}. Contours are at -3σ, 3σ, 5σ, 7σ, ..., where $\sigma = 0.04$ Jy beam^{-1} km s^{-1} for CO(1–0) and $\sigma = 0.114$ Jy beam^{-1} km s^{-1} for CO(3–2). The ALMA beam size is shown lower left and the continuum point source location is shown by the black cross.

A velocity gradient from 50 km s^{-1} at large radii to −100 km s^{-1} coincident with the nucleus is observed along the inner 1 arcsec (1.9 kpc) of the SW filament. This gradient may reverse at larger radii or the outer part of the SW filament may be breaking up or a separate structure. The velocity structure of the SW filament appears to link continuously to the gas projected across the nucleus with a peak at -64 ± 8 km s^{-1} and this structure may extend to include the −150 km s^{-1} gas at the base of the N filament. The SE and N filaments appear clumpy towards the galaxy centre with no clear velocity gradient across the nucleus. However, the additional broad velocity component at the centre suggests there could be a superposition of fainter structures at a range of velocities. The CO(1–0) observations are consistent with this velocity structure but at lower spatial resolution (Fig. 3).

3.5 Molecular gas mass

The molecular gas mass can be calculated from the integrated CO(1–0) intensity ($S_{\rm CO}\Delta v$) under the assumption of a Galactic CO-to-H_2 conversion factor ($X_{\rm CO}$):

$$M_{\rm mol} = 1.05 \times 10^4 X_{\rm CO} \left(\frac{1}{1+z}\right) \left(\frac{S_{\rm CO}\Delta v}{\rm Jy\ km\ s^{-1}}\right) \times \left(\frac{D_{\rm L}}{\rm Mpc}\right)^2 {\rm M}_\odot, \quad (1)$$

where $X_{\rm CO} = 2 \times 10^{20}$ cm^{-2} (K km s^{-1})$^{-1}$ in the Milky Way disc (Solomon et al. 1987; Solomon & Vanden Bout 2005; Bolatto, Wolfire & Leroy 2013), $D_{\rm L}$ is the luminosity distance, and z is the redshift of the BCG. However, the Galactic conversion factor is not expected or observed to be universal (e.g. Narayanan et al. 2011; Bolatto et al. 2013), and likely depends on many environmental factors such as the gas metallicity (e.g. Wilson 1995; Arimoto, Sofue & Tsujimoto 1996; Bolatto et al. 2008). *Chandra* observations show that the cluster atmosphere on the scales of the BCG, from which the molecular gas likely cooled, has subsolar metallicity of $0.4\,{\rm Z}_\odot$ with only modest spatial variations (Sanders et al. 2014). Low metal abundance likely results in an underestimate of the molecular gas mass in PKS 0745−191, unless the cool gas in the filaments has a higher metallicity compared to the ambient ICM (e.g. Panagoulia, Fabian & Sanders 2013).

However, *Spitzer* observations measure an IR luminosity for the BCG just below the $10^{11}\,{\rm L}_\odot$ threshold for a luminous infrared galaxy (LIRG) and starburst galaxies are known to have $X_{\rm CO}$ factors lower than found for galaxy discs. Although the BCG in PKS 0745−191 falls short of the massive starbursts found in ULIRGs, the molecular gas mass could be overestimated by a factor of a few (Solomon et al. 1997; Downes & Solomon 1998). For kinematically disturbed and turbulent gas associated with outflows where the gas may be optically thin even lower $X_{\rm CO}$ factors are expected (for a review see Bolatto et al. 2013). Although the molecular gas in PKS 0745−191 is not settled in the gravitational potential well, the gas velocities are low. The velocity dispersions of the molecular clouds are narrow <6 km s^{-1} (David et al. 2014; Tremblay et al., in preparation), which is typical of an individual molecular cloud in the Galactic disc. In summary, none of these factors suggest that the $X_{\rm CO}$ factor for the BCG in PKS 0745−191 is anomalous and the low metal abundance suggests the molecular gas mass could be underestimated. Our conclusions are not qualitatively altered by the estimated factor of a few uncertainty.

From the integrated CO(1–0) intensity of 2.2 ± 0.1 Jy km s^{-1} (Table 1), the total molecular gas mass is $(4.6 \pm 0.3) \times 10^9\,{\rm M}_\odot$. Roughly one-third of this mass is unresolved within the central peak close to the nuclear continuum emission. Assuming the CO(1–0) and CO(3–2) emission are distributed similarly (Section 3.2), we can estimate the molecular gas mass of each filament. The SE filament is likely the most massive with $\sim 1.9 \times 10^9\,{\rm M}_\odot$. The N

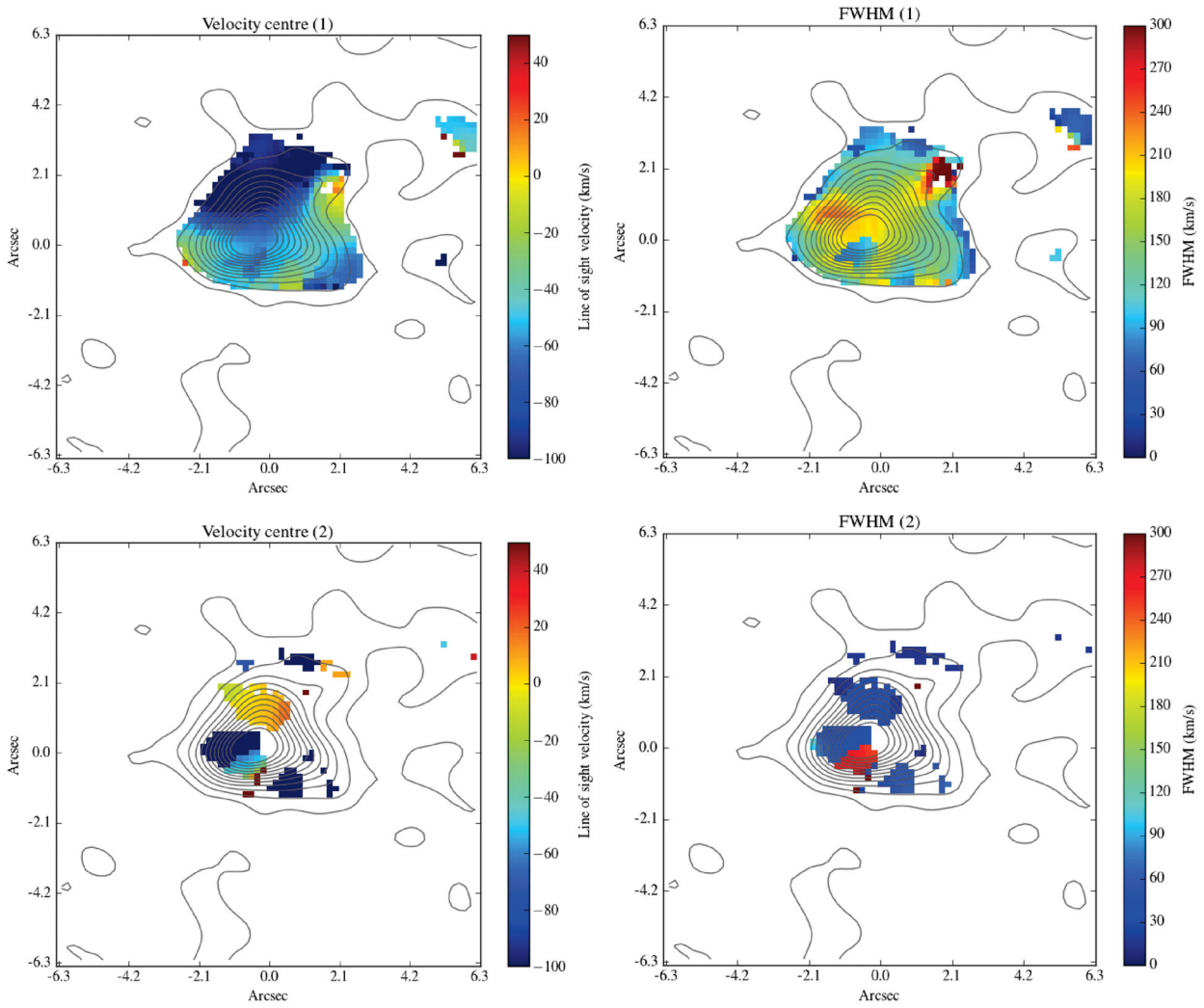

Figure 3. Maps of the CO(1–0) velocity centre (left) and FWHM (right) for each velocity component (1 and 2, where components with similar velocity centres have been grouped together). The image is centred on the nuclear continuum emission (Section 2) and contours from the integrated CO(1–0) intensity map at $1\sigma, 3\sigma, 5\sigma, \ldots$, are shown overplotted. Spectra for the regions to the N and SE of the nucleus that require two velocity components are shown in Fig. 6.

and SW filaments have similar total masses with 1.5×10^9 and $1.3 \times 10^9\,M_\odot$, respectively. Although the CO(3–2) emission appears more centrally concentrated with ∼45 per cent of the total flux within a radius of 0.8 arcsec (comparable to the CO(1–0) synthesized beam), this may indicate that some extended structure has been resolved away rather than intrinsic differences in the spatial distribution.

3.6 Star formation in the BCG

Assuming that CO(3–2) emission traces the gas surface area, the molecular gas surface density of $\sim 800\,M_\odot\,pc^{-2}$ for the BCG is comparable to that of circumnuclear starburst galaxies (e.g. Kennicutt 1998; Daddi et al. 2010; Kennicutt & Evans 2012). *HST* FUV observations show a clear UV excess at the centre of the BCG extending to the W of the nucleus that is clearly coincident with the inner part of the SW filament before it bends at ∼1 arcsec radius (Fig. 9). The SBC *F140LP* observation does not suffer from contaminating line emission or a significant AGN contribution (Quillen et al. 2008; Donahue et al. 2011; Mittal, Whelan & Combes 2015). The cold molecular gas filament extending to the SW is therefore coincident with a recent burst of star formation whilst the other two filaments lie along dust lanes with little star formation detected in the FUV (Fig. 9). The dust lanes may obscure star formation in the N and SE molecular filaments but the agreement between the FUV and IR-derived star formation rates suggests no significant population of buried young stars (Johnstone et al. 1987; Romanishin 1987; Hicks & Mushotzky 2005; O'Dea et al. 2008; Donahue et al. 2011; Mittal et al. 2015). *Spitzer* infrared photometry and spectroscopy reveal star formation rates of $17\,M_\odot\,yr^{-1}$ (O'Dea et al. 2008) and $11\,M_\odot\,yr^{-1}$ (Donahue et al. 2011), respectively. Using the extent of the CO(3–2) emission in the SW filament, the star formation surface density is $\sim 6\,M_\odot\,yr^{-1}\,kpc^{-2}$. The BCG in PKS 0745−191 therefore lies on the Kennicutt–Schmidt relation with IR-selected starburst galaxies (Kennicutt 1998; Kennicutt & Evans 2012).

4 DISCUSSION

4.1 Origin of the molecular gas

The inferred molecular gas mass in the BCG is substantially higher than that typically found in early-type galaxies raising the question

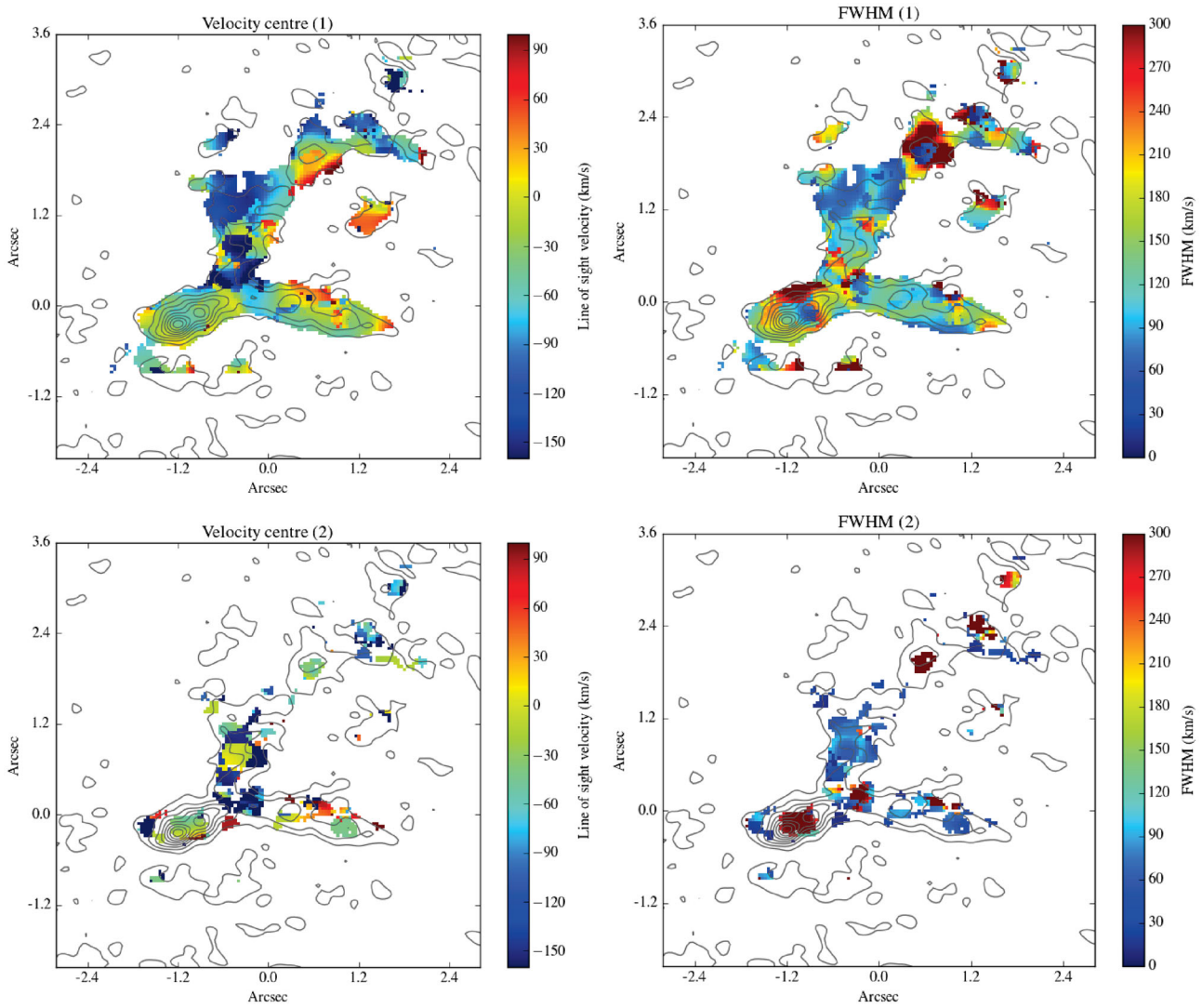

Figure 4. Maps of the CO(3–2) velocity centre (left) and FWHM (right) for each velocity component (1 and 2, where components with similar velocity centres have been grouped together). The origin is located at the position of the nuclear continuum emission (Section 2) and contours from the integrated CO(3–2) intensity map at $1\sigma, 3\sigma, 5\sigma, \ldots$, are shown overplotted. Spectra for regions in each filament requiring two velocity components are shown in Fig. 7.

of its origin. Mergers between the BCG and donor galaxies are likely rare due to the dearth of gas-rich galaxies at the centres of rich clusters (e.g. Young et al. 2011) and because the cluster's high-velocity dispersion decreases the merger rate. Ram pressure stripping by the ICM of a gas-rich galaxy that passes close to the BCG seems similarly unlikely. Molecular gas is much more tightly bound to its host galaxy than atomic gas and is retained on all but the most eccentric orbits within a cluster (e.g. Young et al. 2011). Observations of Virgo cluster members have shown that galaxies with strong H I deficiencies have minimal molecular gas deficiencies (Kenney & Young 1989; di Serego Alighieri et al. 2007; Grossi et al. 2009). In PKS 0745−191, the filaments have low velocities, radial morphologies and shallow velocity gradients with no indication of the high velocities and large-scale rotation expected from the stripping of a merging galaxy (e.g. Ueda et al. 2014). The three observed filaments in the BCG would likely require separate direct impacts by gas-rich galaxies each depositing similarly large quantities of molecular gas at low velocities.

BCGs located at the centres of dense cluster atmospheres with radiative cooling times below a gigayear are known to host cold molecular gas in excess of a few $\times 10^9\,M_\odot$ (Edge 2001; Salomé & Combes 2003). The Perseus cluster hosts $4 \times 10^{10}\,M_\odot$ of extended molecular gas filaments coincident with the coolest X-ray gas (Salomé et al. 2006). The simplest interpretation of their velocity structure is an inflow of gas cooling from the ICM, free-falling towards the BCG (Lim et al. 2008; Salomé et al. 2008). In PKS 0745−191, the X-ray cooling rate of $270 \pm 90\,M_\odot\ \mathrm{yr}^{-1}$ determined from *XMM*-RGS spectroscopy (Sanders et al. 2014) could supply the molecular gas mass in only ∼20 Myr. This cooling time-scale is also comparable to the time since the last major AGN outburst given by the age of the X-ray cavities, which require ∼10–20 Myr to rise at the sound speed to the observed projected radii (Rafferty et al. 2006; Sanders et al. 2014). Whilst, it appears likely that the molecular gas cooled from the cluster atmosphere, the low gas velocities are inconsistent with free-fall.

4.2 Molecular gas clouds in gravitational free-fall?

The velocity gradients detected in the N and SW filaments could indicate an inflow of gas cooling from the cluster atmosphere but

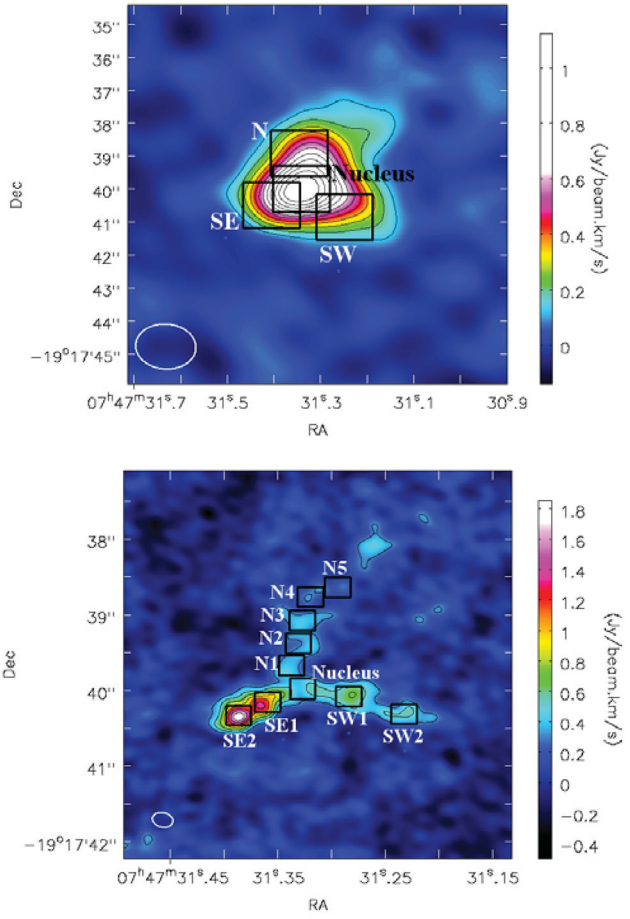

Figure 5. PKS 0745−191 CO(1–0) (top) and CO(3–2) (bottom) integrated intensity maps (as shown in Fig. 2) with regions overlaid corresponding to the spectra shown in Figs 6 and 7.

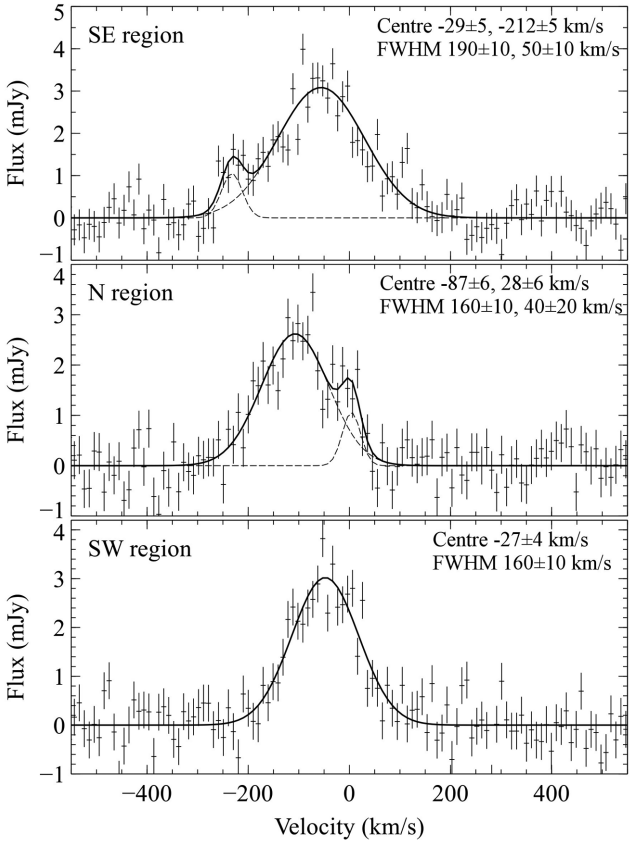

Figure 6. CO(1–0) spectra from regions requiring two velocity components and a comparison region to the SW. The best-fitting model is shown by the solid line and individual Gaussian components are shown by the dashed lines. The best-fitting parameters are given in Table 1.

the interpretation depends on the location of the gas along the line of sight. Without absorption line observations showing whether the cold gas lies in front or behind the galaxy, it is difficult to unambiguously determine whether gas is moving in or out. However, the low velocities and shallow velocity gradients are inconsistent with simple models for gas cooling steadily from the cluster atmosphere. The ICM is approximately in hydrostatic equilibrium; therefore, an overdense, rapidly cooling gas blob is initially at rest with respect to the cluster. This cooling gas decouples from the cluster atmosphere and is expected to subsequently free-fall in the cluster's gravitational potential (e.g. Pizzolato & Soker 2005, 2010; Gaspari et al. 2015). Although X-ray gas pressure and cloud–cloud collisions will slow the infall, in general we expect a smooth radial velocity gradient with the highest velocities at the smallest radii. The velocity gradients along the SW and N filaments steadily increase to −100 and −200 km s^{-1} with decreasing radius over a distance of a few kpc, respectively. The SE filament may have a similar velocity gradient obscured by an orientation close to the line of sight.

Following Lim et al. (2008), we assume a Hernquist model for the gravitational potential of an elliptical galaxy, expressed in terms of the total mass and effective radius, that reproduces a de Vaucouleurs surface brightness profile (Hernquist 1990). The velocity of a gas blob that free-falls in this potential is given by

$$v(r)^2 = v(r_0)^2 + 2GM\left(\frac{1}{r+a} - \frac{1}{r_0+a}\right), \quad (2)$$

where M is the total galaxy mass, a is the scale radius, which is related to the effective radius $R_e \sim 1.8153a$, r_0 is the initial radius and $v(r_0)$ is the initial velocity. For PKS 0745−191, Allen, Fabian & Kneib (1996) measured a projected mass within a radius of 34 kpc of $1.8 \times 10^{13}\,M_\odot$ using a strong gravitational lensing analysis (corrected for our cosmology, see also Sanders et al. 2014). However, X-ray mass estimates assuming hydrostatic equilibrium have measured a lower total mass of $\sim 2 \times 10^{12}\,M_\odot$ within a radius of 30 kpc (Voigt & Fabian 2006; Sanders et al. 2014). The X-ray mass may be affected by strong deviations from spherical symmetry or a breakdown of hydrostatic equilibrium in the cluster centre. We have considered both estimates of the total mass in our analysis. The scale radius of 10 kpc was estimated from the K-band effective radius of 9.5 arcsec given by the Two Micron All Sky Survey (2MASS) extended source catalogue[2] (Skrutskie et al. 2006). We note that this may underestimate the true value as the 2MASS observations are not deep enough to trace the full extent of the BCG envelope and PKS 0745−191 lies near the Galactic plane on the sky.

The remaining free parameters are the initial radius, where the gas blob starts to free-fall, and the inclination to the line of sight. Beyond ∼0.5 arcsec (∼1 kpc) from the initial radius, the velocity increases linearly with decreasing radius therefore the inclination is the main parameter that can be altered to match the velocity

[2] http://www.ipac.caltech.edu/2mass

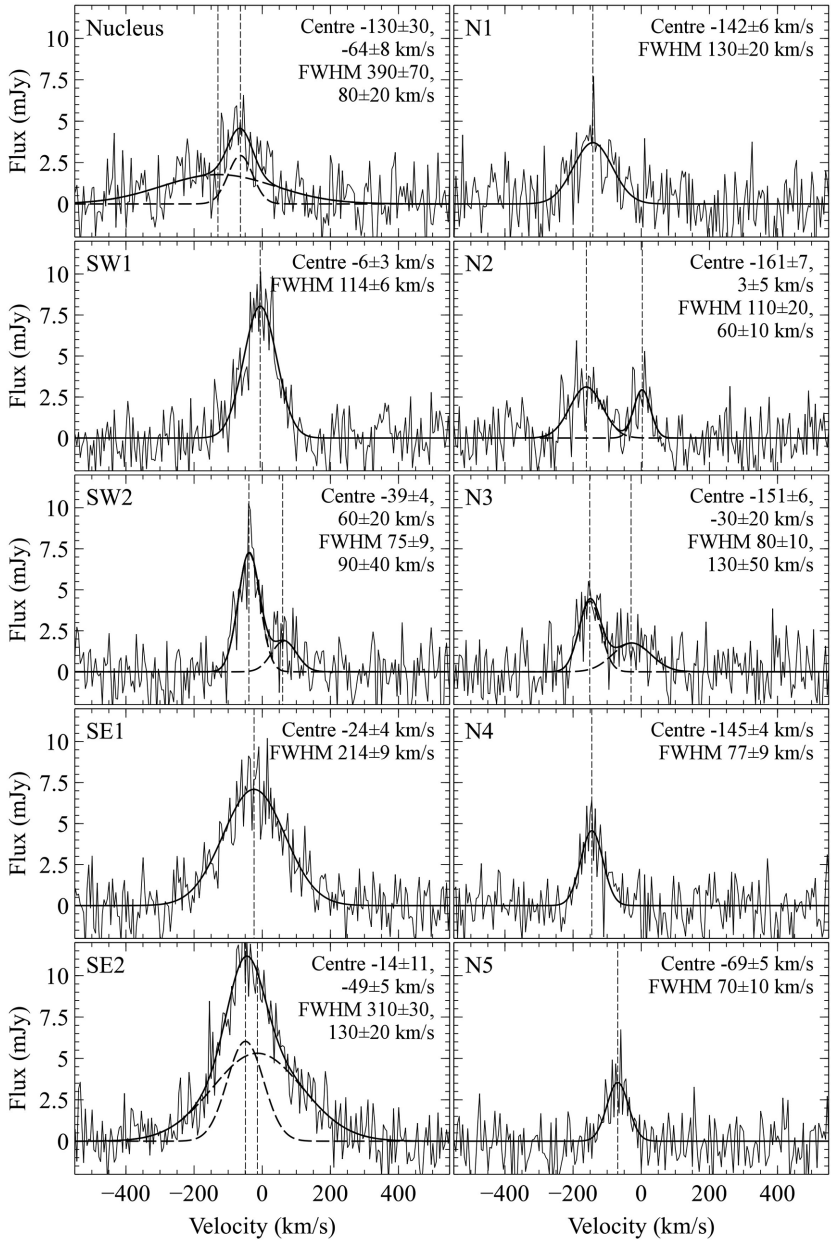

Figure 7. CO(3–2) spectra for beam-sized regions along each filament with low numbers at small radii. The line centres are marked with vertical dashed lines for comparison.

structure. However, for both the N and SW filaments, the shallow velocity gradients require an orientation $<20^\circ$ from the plane of the sky. This assumes the conservative X-ray estimate of the total mass. The gravitational lensing total mass requires an even more stringent orientation $<10^\circ$ from the plane of the sky.

The low velocities of the cold gas found in all three filaments appear inconsistent with gravitational infall. For an orientation of 30° from the plane of the sky, a gas blob released from rest at a projected radius of 2 arcsec (3.8 kpc) will reach a velocity of $\sim$250 km s^{-1} over 1 arcsec projected distance. Depending on the exact form of the gravitational potential, the expected free-fall velocities could be higher by a factor of 2. Therefore, if the molecular gas structures originated more than a few kpc from their current locations their velocities should significantly exceed those observed. The velocity of an infalling gas blob may be slowed by ram pressure drag from the ICM, although this is expected to be a minor effect for such dense gas, or by cloud–cloud collisions inside a radius of $\sim$1 kpc (e.g. Pizzolato & Soker 2005; Gaspari et al. 2015). Cloud–cloud collisions could be producing the broader FWHM at the base of the N filament where it may intersect the other filaments but are unlikely to substantially reduce the gas velocities at larger radii. For such low velocities and narrow FWHM, the molecular filaments must be transient structures formed from gas cooling locally and supported *in situ* (see Section 4.5).

If the molecular filaments formed from rapid cooling of the hot atmosphere, the lack of molecular gas that could be associated with a previous cooling episode appears inconsistent with the observed stability of AGN feedback. The prevalence of short central radiative cooling times in cluster atmospheres and strong correlations with detections of cold gas, star formation and H α emission suggest that

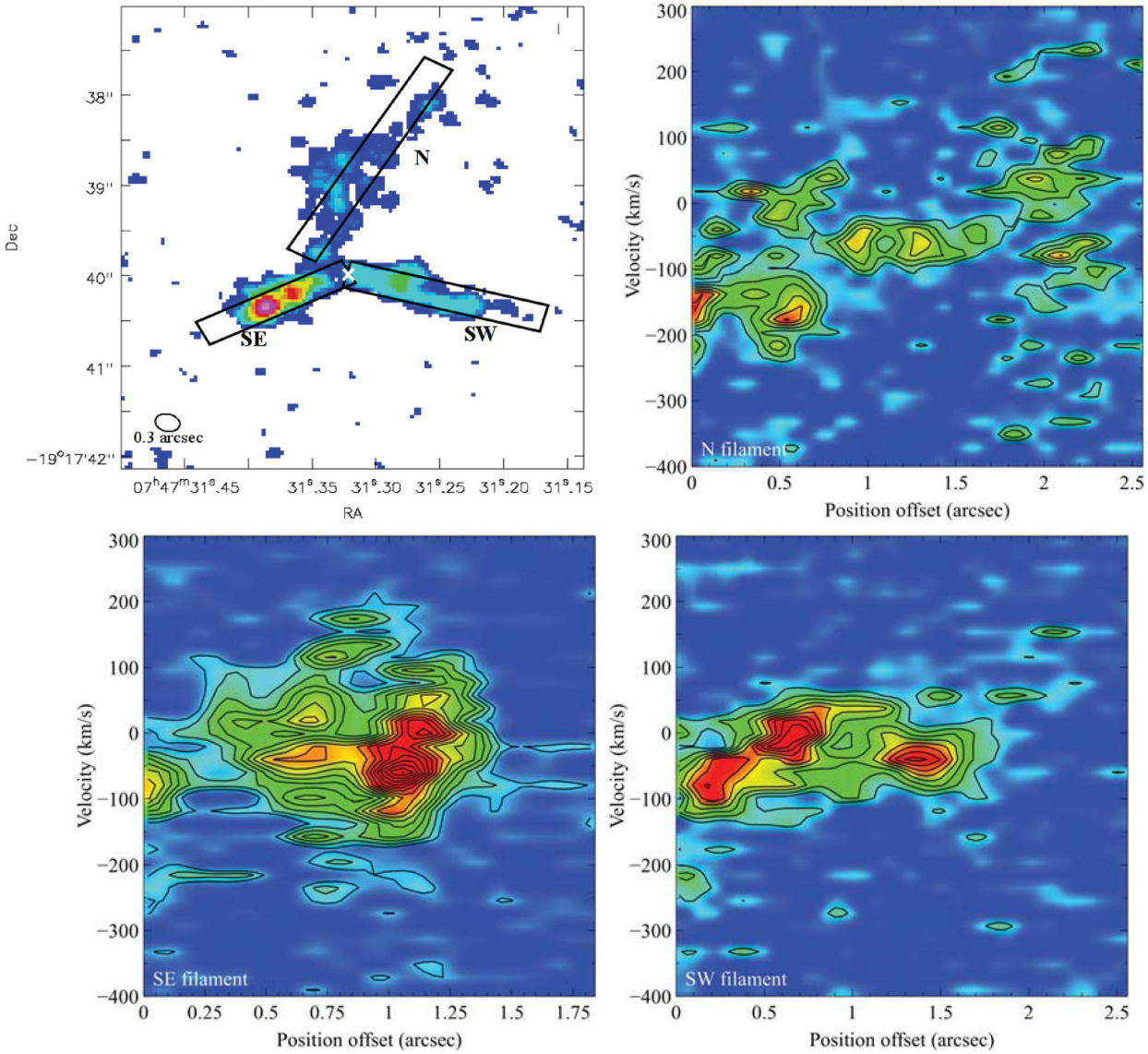

Figure 8. Position velocity diagrams for each of the CO(3–2) filaments with the CO(3–2) integrated intensity map overlaid with the location of each PV slit shown upper left. The position offset is minimum closest to the nucleus for each diagram. Contours are 2σ, 3σ, 4σ etc. The nuclear continuum point source location is shown by the cross (Section 2).

cooling is long-lived (Fabian 2012; McNamara & Nulsen 2012). Studies of the fraction of cool core clusters with radio bubbles and central radio sources suggest that the duty cycle of AGN activity in BCGs is at least 70 per cent (Dunn & Fabian 2006, 2008; Bîrzan et al. 2012). AGN feedback appears more or less continuous, rather than strongly episodic, and the good agreement between the radio power and cooling losses suggest a stable balance to $z \sim 0.7$ (e.g. Ma et al. 2011; Hlavacek-Larrondo et al. 2012). Repeated episodes of cooling and heating in PKS 0745−191 are more consistent with these observations than a single, sudden influx of cold gas on to the BCG. Rapid accretion of previous massive molecular inflows by the SMBH would require implausibly high efficiency forming few young stars in the process.

4.3 Outflowing molecular gas clouds?

The most significant dust lane features detected in the BCG in *HST* observations (Fig. 9; Donahue et al. 2000) lie along the N and SE filaments. If the dusty molecular gas clouds obscured more than ∼50 per cent of the galaxy light then blueshifted and redshifted gas components could be cleanly interpreted as outflow and inflow, respectively. Using the *F555W HST* image, we subtracted the average surface brightness determined in sectors free of emission lines and dust in a series of elliptical annuli. The ellipticity and P.A. for the BCG were taken from the 2MASS extended source catalogue (Skrutskie et al. 2006) and should therefore not be affected by the line emission and dust lane structure. Along the dust lanes coincident with the N and SE filaments, the surface brightness falls 20–50 per cent below the average at that radius. The SW filament is instead coincident with excess emission at 20–40 per cent above the average at each radius likely due to star formation.

The peak absorbed fraction in the N and SE filaments could be higher as they are likely composed of unresolved dense, giant molecular cloud associations producing variations in the covering fraction on unresolved spatial scales in the *HST* images (e.g. Salomé et al. 2008, 2011; David et al. 2014). In NGC 1275, Salomé et al. 2008

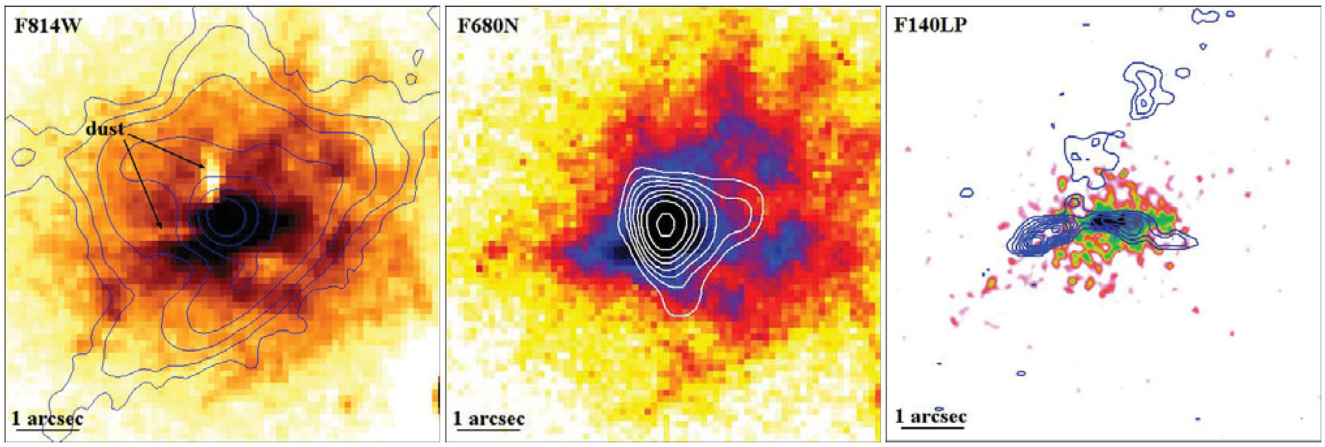

Figure 9. Left: *HST F*814*W* image of the BCG showing the old stellar population and H α+[NII] emission (Sand et al. 2005; Mittal et al. 2015; Tremblay et al. 2015). A smooth model has been subtracted to show the dust lanes extending to the N and E of the nucleus. Contours show the 5 GHz VLA radio emission from Baum & O'Dea (1991). Centre: Narrow band image covering the H α+[NII] emission (Donahue et al. 2000) with the 14.9 GHz VLA B array contours overlaid (Baum & O'Dea 1991). Right: *F*140*LP* SBC image of FUV continuum emission from massive, young stars (Mittal et al. 2015; Tremblay et al. 2015) with ALMA CO(3–2) integrated intensity contours overlaid. All images are centred on the nuclear continuum point source emission (Section 2).

found that the CO line ratios indicate optically thick radiation but the observed brightness temperature of the molecular gas clumps is at least an order of magnitude below the expectation for normal, optically thick clouds. These observations can be reconciled if each molecular clump is comprised of many giant molecular clouds each with a mass of $\sim 10^6\,M_\odot$ and a radius of $\sim$30 pc typical of those found in the Milky Way (Solomon et al. 1987). Although the complexity of the structure makes a clean interpretation difficult, it is plausible that the peak absorbed fraction is significantly higher and therefore the bulk of the molecular gas in the NW and SE filaments lies on the near side of the galaxy. Regions of $\sim$50 per cent absorption in the N and SE filaments show that some of the gas clouds lie in front of the galaxy mid-plane.

Both velocity components in the SE filament are blueshifted with respect to the BCG's systemic velocity and may be flowing away from the galaxy centre. Whilst, the brightest velocity component at CO(1–0) has only a small velocity shift to -29 ± 5 km s^{-1}, the second component is clearly observed as a blueshifted wing at -212 ± 5 km s^{-1}. Although two velocity components are detected in the SE filament in the CO(3–2) emission, the velocities are modest, perhaps indicating different gas properties in this outflowing component. Blueshifted and redshifted velocity components are detected in the N filament at both CO(1–0) and CO(3–2). Multiple coincident velocity components likely indicates a superposition of structures along the line of sight. The more massive blueshifted component presumably lies in front of the galaxy centre and may similarly indicate gas outflowing from the galaxy centre. The second, less massive velocity component is redshifted to at most 28 ± 6 km s^{-1} and is projected close to the nucleus but may lie anywhere along the line of sight.

In summary, the velocity structure and dust obscuration observed in the N and SE filaments are consistent with the bulk of the molecular gas moving outwards from the galaxy centre.

4.4 Molecular gas clouds lifted by radio bubbles?

Radio and X-ray observations suggest that radio jet outbursts from the central SMBH are interacting with the extended molecular and ionized gas filaments. The Very Large Array (VLA) 14.9 GHz observation with a resolution of $\sim$0.15 arcsec shows a bright nucleus with an extension of the radio emission 0.5 arcsec in length to the W (Fig. 9; Baum & O'Dea 1991). The bright radio nucleus is coincident with the continuum point source detected with ALMA in the submm and a hard X-ray point source detected with *Chandra*. A jet may have disrupted in the dense cluster environment, which is consistent with the amorphous radio appearance. Other radio galaxies in dense cluster environments are similarly disrupted, such as PKS 1246−410 at the centre of the Centaurus cluster (Taylor et al. 2006). This more diffuse structure observed in PKS 0745−191 in 1−2 GHz VLA images extends towards two X-ray surface brightness depressions, each $\sim$20 kpc across, located to the N and SE in *Chandra* observations (Fig. 10; Rafferty et al. 2006; Sanders et al. 2014). The AGN has inflated two large radio bubbles detected as cavities in the X-ray emission where the radio lobes have displaced the cluster's hot atmosphere (McNamara & Nulsen 2007, 2012; Fabian 2012).

The N and SE molecular filaments extend out towards the X-ray cavities and may have been lifted from the galaxy in the wake of the buoyantly rising bubbles. No clear cavity is detected near the SW molecular gas filament although this would be difficult to detect under the bright soft X-ray ridge of emission. A small, young cavity may be located between the ridge and the X-ray point source where the X-ray surface brightness drops. ALMA observations of the BCG at the centre of A1835 have found a $10^{10}\,M_\odot$ bipolar molecular flow in similarly extended filaments that may be accelerated outwards by the mechanical energy associated with rising radio bubbles (McNamara et al. 2014). Single dish detections of molecular gas coincident with H α filaments beneath buoyant radio bubbles in the Perseus cluster are consistent with this scenario (Salomé et al. 2006, 2011). Radio jet-driven outflows of molecular gas have also been detected in nearby galaxies (e.g. Alatalo et al. 2011; Tadhunter et al. 2014; Morganti et al. 2015). Using a total molecular gas mass of $5 \times 10^9\,M_\odot$, a gas velocity of 100 km s^{-1} and velocity dispersion of 100 km s^{-1}, the energy required to accelerate the molecular gas is several $\times 10^{57}$ erg. By calculating the 4*PV* work done inflating the two radio bubbles in the hot atmosphere, Sanders et al. (2014) estimated that the AGN outburst supplies $\sim 3 \times 10^{60}$ erg, which is energetically sufficient to uplift the molecular gas.

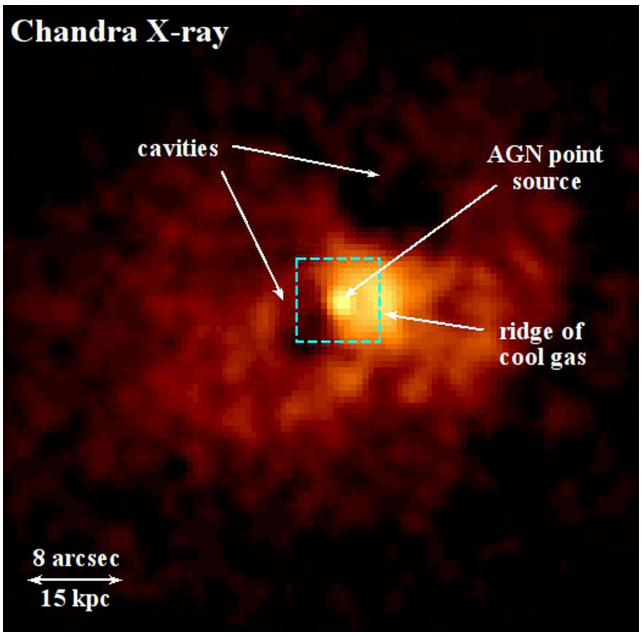

Figure 10. *Chandra* X-ray image (0.3–7 keV) of the hot atmosphere surrounding the BCG in PKS 0745−191. A smooth X-ray background has been subtracted. The box corresponds to the region covered by the optical images in Fig. 9.

Buoyant bubbles cannot lift more weight than they displace. Using a conservative estimate of the surrounding gas density, the radio bubbles displace $\sim 5 \times 10^{10}$ M$_\odot$ of hot gas and therefore could have lifted 5×10^9 M$_\odot$ of molecular gas along with a significant amount of warmer gas.

The NW and SE filaments in PKS 0745−191 comprise 60–70 per cent of the total cold molecular gas, which suggests very strong coupling to the radio bubbles. The lack of any centrally concentrated reservoir of molecular gas coincident with the nucleus requires an even higher coupling fraction. It is difficult to understand how radio bubbles could uplift dense molecular gas clouds so efficiently. Volume-filling gas would be easier to lift. Roughly 20 per cent of the molecular gas appears uplifted by the radio bubbles in A1835, which together with the hot gas outflow produces a total uplifted mass uncomfortably close to the theoretical maximum. McNamara et al. (2014) suggested that turbulence maintained by ongoing star formation would reduce the density contrast and enable uplift of the molecular gas by the hotter gas. However, the star formation in PKS 0745−191 is concentrated in the SW filament.

4.5 Forming molecular gas in extended filaments

In a cluster atmosphere where AGN heating locally balances radiative cooling, uplift by radio bubbles can promote cooling by removing gas from this equilibrium state. Low entropy gas that has been lifted to larger radii is cooler and denser than the surroundings and therefore radiates more energy than can be replaced by the local heating rate. The molecular gas filaments could therefore have formed from warmer gas that was uplifted by the radio bubble and cooled locally (Churazov et al. 2001; Revaz, Combes & Salomé 2008; Li & Bryan 2014). Rapid cooling of shock-heated outflowing gas to form molecules on short time-scales has been suggested to explain the molecular gas kinematics in IC 5063 and 4C 12.50 (Morganti et al. 2013; Tadhunter et al. 2014; Zubovas & King 2014; Morganti et al. 2015). Fig. 9 shows that the molecular gas filaments also trace the brightest regions of optical line emission and this gas is coincident with low-temperature X-ray gas (Sanders et al. 2014). The time taken for the radio bubbles to rise at the sound speed to the observed projected radii is ∼10 Myr for the E bubble and ∼20 Myr for the NW bubble. The X-ray cooling rate of 270 ± 90 M$_\odot$ yr^{-1} is large enough to supply the inferred molecular gas mass of the filaments in this time (Section 4.1). This would however require catastrophic cooling of the hot gas around the radio bubbles. From Sanders et al. (2014), the hot gas density profile within ∼20 kpc radius can be approximated by a power-law $\rho \propto r^{-1}$. Extrapolating into the cluster centre, the hot gas mass is $\sim 4 \times 10^9$ M$_\odot$ within a sphere of radius 5 kpc, which covers the extent of the molecular filaments. Rapid cooling to supply the $\sim 5 \times 10^9$ M$_\odot$ of molecular gas would therefore deplete the hot gas at the cluster centre and the resulting inflow would oppose uplift of the gas.

The slowest step in the cooling process is the formation of molecular hydrogen, which requires the presence of dust grains to occur on these time-scales (e.g. Ferland, Fabian & Johnstone 1994; Ferland et al. 2009). Dust grains are sputtered rapidly (<1 Myr) in the X-ray atmosphere (Draine & Salpeter 1979; Dwek & Arendt 1992) so cooling X-ray gas is likely dust-free. However, the N and SE molecular filaments are clearly coincident with dust lanes in the *HST* observations (Fig. 9). Little recent star formation is detected in these filaments but dust could have been distributed locally by the BCG's older stellar population. Material ejected from stars at the centres of cool core clusters may not necessarily mix rapidly with and be heated by the surrounding hot gas environment (Voit & Donahue 2011). If this gas remains cool, the embedded dust will be preserved and could enrich the cooling gas filaments. The dusty molecular wake extending 4 pc behind the evolved star Mira in our galaxy suggests that stellar ejecta can remain cold and dense in the interstellar medium, consistent with this scenario (Martin et al. 2007). Dust could also have been uplifted from the BCG centre along with the rapidly cooling gas and shielded from the X-ray atmosphere in dense gas clumps. If the molecular gas has the momentum of the warmer, uplifted gas that it cooled from, the low outflow velocities suggest a gentle acceleration that would not destroy dust grains. Slow entrainment of the gas by the radio bubbles would also not dissociate the molecular gas.

For the observed gas velocities of ± 100 km s^{-1} and projected lengths of 3-5 kpc, the dynamical ages of the SE and N filaments are $1–2 \times 10^7$ yr, which is approximately the bubble rise time. However, if the molecular filaments are only supported by thermal pressure, they would collapse under tidal gravitational forces on time-scales <1 Myr (e.g. Ho, Lim & Dinh-V-Trung 2009). The survival of dense gas filaments at the centres of hot, high-pressure cluster atmospheres for at least a dynamical time-scale suggests that magnetic fields are required to support and insulate against rapid evaporation. This assumes that the small ionized fraction of the cold gas supported by the magnetic field effectively transmits the magnetic stress to the large neutral portion through collisions. Ambipolar diffusion is also assumed to be sufficiently slow to allow effective links between the molecular, atomic and ionized gas components (e.g. Shu 1992; McKee & Ostriker 2007). Fabian et al. (2008) show that the thread-like H α filaments in the Perseus cluster are likely supported by magnetic fields of at least a few tens of μG (see also Ho et al. 2009). The filamentary structure of the molecular gas and optical line emission in PKS 0745−191 appears very

similar to the Perseus cluster. The molecular gas filaments are likely to be a superposition of many separate structures and unresolved strands.

However, the demands on magnetic support appear much greater in PKS 0745−191. The magnetic pressure required to support the molecular gas is $P_{\rm B} \sim B^2/8\pi \sim \Sigma g$, where B is the magnetic field strength, Σ is the molecular gas surface density and g is the gravitational acceleration. The width of each filament in PKS 0745−191 is not resolved therefore we calculate a lower limit on the magnetic pressure by assuming that the width is given by the synthesized beam. The SE filament is ∼3 kpc in length with a radius of 0.3 kpc and a molecular gas mass of $1.9 \times 10^9\,{\rm M}_\odot$. Following Fabian et al. (2008), for a radial filament the lengthwise column density $N \sim 7 \times 10^{23}$ cm^{-2} and the surface density $\Sigma_\parallel \sim 1.2$ g cm^{-2}. The gravitational acceleration at the centre of PKS 0745−191 $g \sim 10^{-8}$ cm s^{-2} (Sanders et al. 2014). The magnetic pressure required $P_{\rm B} \sim 1.2 \times 10^{-8}$ erg cm^{-3}, which is roughly an order of magnitude greater than the thermal pressure of the hot gas $P_{\rm T} \sim 8 \times 10^{-10}$ erg cm^{-3} (Sanders et al. 2014). Therefore, supporting the weight of the massive cold gas filament requires a magnetic pressure that substantially exceeds the hot gas pressure. The corresponding magnetic field strength $B \sim 400\,\mu$G is significantly above typical values for cluster cores (Carilli & Taylor 2002; Govoni & Feretti 2004) and possible enhancements from flux-freezing (e.g. Sharma, Parrish & Quataert 2010). Such a large, aspherical pressure distribution in the cluster centre should produce departures from hydrostatic equilibrium in the hot gas. Sanders et al. (2014) found evidence for non-thermal pressure within a radius of 40 kpc in PKS 0745−191 and showed that the coolest X-ray emitting gas is offset by around 5 kpc from the nucleus. This asymmetry could be related to sloshing of the cool core (Sanders et al. 2014) or, for a magnetically dominated core, it could indicate clumping of the hot gas as the ICM is squeezed by the magnetic pressure. The hot gas in the cluster centre will therefore have a low filling factor and a lower mean density compared to a uniformly distributed medium. The amorphous structure of the central radio source is coincident with and may be related to this magnetically dominated core region. Faraday rotation measurements of the extended radio emission could be used to determine the magnetic field strength.

The problems of magnetic pressure support and hot gas depletion could be alleviated if the $X_{\rm CO}$ factor for BCGs, and correspondingly the molecular gas mass, was lower by an order of magnitude. For a lower molecular gas mass of $\sim 5 \times 10^8\,{\rm M}_\odot$, the magnetic pressure required to support the filaments would be comparable to the hot gas pressure, consistent with the X-ray observations (Sanders et al. 2014). Rapid cooling of only 10 per cent of the hot gas within a radius of 5 kpc could supply the molecular gas mass on the required time-scales. A reduced $X_{\rm CO}$ factor would also not move the filaments in PKS 0745−191 significantly beyond the scatter of the Kennicutt–Schmidt relation (e.g. Kennicutt & Evans 2012). ULIRG and starburst galaxy environments are known to have kinematically disturbed molecular gas with higher temperatures and velocity dispersions causing reductions in $X_{\rm CO}$ by a factor of a few to ten (e.g. Solomon et al. 1997; Downes & Solomon 1998; Bolatto et al. 2013). However, as discussed in Section 3.5, the low gas velocities in PKS 0745−191 and narrow velocity dispersions observed for molecular clouds in BCGs are inconsistent with the conditions in starburst galaxies. Herschel observations tracing the dust emission in PKS 0745−191 show that the bulk of the dust is low temperature at ∼25 K and a Galactic $X_{\rm CO}$ factor produces a gas-to-dust mass ratio of ∼100 consistent with that found in the Milky Way (Oonk et al., in preparation). Therefore, whilst a lower $X_{\rm CO}$ factor could alleviate several problems, we find no clear evidence to support a significantly lower value in PKS 0745−191 beyond galaxy-to-galaxy variations. The low metal abundance suggests the molecular gas mass could instead be underestimated unless the cool gas in the filaments has an enhanced metallicity over the ambient ICM (e.g. Panagoulia et al. 2013).

4.6 Fate of the molecular gas

Fig. 9 shows a striking coincidence between the SW filament of molecular gas, a spur of young, massive stars in the FUV and extended radio emission detected at 7σ significance in 14.9 GHz VLA observations (Baum & O'Dea 1991). The filament also extends towards the surface brightness peak of the cluster emission. In comparison, little recent star formation is observed coincident with either the N or SE filaments even though each has a higher inferred molecular gas mass and similar velocity structure. An external perturbation, such as an expanding radio structure, may have triggered gas cloud collapse and star formation in the SW filament. The dust lanes coincident with the N and SE filaments could obscure recent star formation, although IR observations are inconsistent with a substantial population of buried young stars (Section 3.6) and it is not clear why the SW filament is not similarly dusty.

A collision between an expanding radio lobe and dense gas clouds in the SW filament may have disrupted the radio structure and triggered star formation at this location, consistent with the amorphous radio morphology in lower frequency observations. Jet-triggered star formation is thought to be occurring in Cen A and Minkowski's object (Graham & Price 1981; van Breugel et al. 1985; Dey et al. 1997; Bicknell et al. 2000; Oosterloo & Morganti 2005; Santoro et al. 2015; Salomé et al. 2016) and could explain the ∼90° deflection of the radio jets in A1795 (McNamara et al. 1996; Pinkney et al. 1996). For A1795, knots of young star clusters and dense molecular gas clouds clearly trace the outer edges of radio lobes and an increase in the ionization state, turbulence and density of the gas at the deflection point in the jets implies a direct interaction (Crawford, Sanders & Fabian 2005). However, although the gas filament appears deflected at the end of the small-scale extension of the radio emission in PKS 0745−191, no increase in the velocity dispersion is observed either along the SW filament or by comparison with the other filaments. The SW filament also has a lower CO(3–2)/CO(1–0) line ratio than the other filaments which is consistent with more diffuse gas. It is therefore not clear if these structures are physically interacting or merely observed as coincident in projection.

Star formation also occurs in a minority of the extended cool gas filaments in the Perseus cluster despite their substantial molecular gas mass (Canning et al. 2014). Only three separate regions of the outer filaments have been disrupted by an unknown mechanism and rapidly collapsed into stars <50 Myr ago (Canning et al. 2014). The filaments do not appear to become generally unstable due to bulk sloshing motions in the ICM or growth through hot gas mixing with the cold phase and weak shocks generated by the radio bubble inflation do not appear to have similarly destabilized the inner filaments (Fabian et al. 2011; Canning et al. 2014). Star formation only in the SW filament in PKS 0745−191 is consistent with these findings and given the comparable structure of the three separate gas filaments it appears likely that the radio structure is responsible for triggering its collapse.

The long-term state of the non-star-forming filaments is unclear. The gas velocities lie far below the BCG's escape velocity therefore the molecular gas clouds will remain in the galaxy's potential. The outer filaments may eventually evaporate in the hot cluster gas or fall back on to the central galaxy and subsequently fuel the AGN. If these cold gas clouds are subsequently fuelling the AGN, the feedback must somehow be prompt or approximately constant to explain the close connection between detections of cold gas, H α emission and star formation and short radiative cooling times in the hot cluster atmosphere (Edge 2001; Salomé & Combes 2003; Cavagnolo et al. 2008; Rafferty et al. 2008). Lower significance structures at the outer sections of the N and SE filaments hint at the break up of these filaments (Fig. 4). Deeper observations will be required to determine the fate of these gas clumps, potentially as a circulation flow falling back to the BCG centre (Salomé et al. 2006, 2011; Lim et al. 2008).

5 CONCLUSIONS

ALMA Cycle 1 observations of PKS 0745−191 have revealed $4.6 \pm 0.3 \times 10^9\,\mathrm{M}_\odot$ of molecular gas in the BCG in three large filaments extending to 3−5 kpc radii. The molecular cloud velocities are remarkably low, within ± 100 km s^{-1} of the BCG's systemic velocity, and the velocity dispersion is significantly less than the typical stellar velocity dispersion of such a massive BCG. Apparently, the molecular gas has not settled into the gravitational potential well and the filament structure is expected to break up on $<10^7$ yr time-scales unless it is supported, possibly by magnetic fields. The low velocities and shallow velocity gradients along the filaments are inconsistent with free-fall or a merger. The molecular gas clouds must have originated from gas cooling less than a few kpc from their current location or much higher velocities would be observed. However, although the X-ray cooling rate from the *XMM*-RGS could supply $\sim 5 \times 10^9\,\mathrm{M}_\odot$ of molecular gas on a 20 Myr time-scale, such rapid cooling would dramatically deplete the hot gas within the $\sim$5 kpc radius of the filaments.

The N and SE filaments are projected beneath cavities in X-ray surface brightness images corresponding to large radio bubbles inflated by the central AGN that are now buoyantly rising through the cluster. These filaments contain 60–70 per cent of the total molecular gas mass, therefore direct uplift by the radio bubbles appears to require an implausibly high coupling efficiency. In a cluster where AGN heating is locally balanced by radiative cooling, lifting low entropy gas from its equilibrium state at the cluster centre can promote cooling. The cold filaments are coincident with low temperature X-ray gas, bright optical line emission and dust lanes suggesting that the molecular gas could have formed by gas cooling from uplifted warmer gas. The survival of these extended cold gas filaments for at least a dynamical time-scale suggests magnetic fields are required for support and insulation against the hot cluster atmosphere. Supporting the weight of the massive molecular filaments requires a magnetic pressure that is an order of magnitude greater than the hot gas pressure. *Chandra* observations of PKS 0745−191 are consistent with departures from hydrostatic equilibrium in the cluster core and non-thermal pressure contributions within a radius of 40 kpc.

The N filament extends furthest and appears to be breaking into clumps at large radius. The filaments may eventually fragment with gas clouds falling back on to the BCG centre in a circulation flow that subsequently fuels the central AGN. However, if the filaments are formed from rapid cooling of the cluster atmosphere at $\sim 200\,\mathrm{M}_\odot$ yr^{-1}, we would expect to detect molecular gas structures associated with previous cooling episodes. The prevalence of short central radiative cooling times in cluster atmospheres and strong correlations with detections of cold gas and star formation suggest that cooling is long-lived and the AGN supplies a regular input of energy. Whilst, a single episode of rapid cooling seems unlikely, it also appears implausible that such a large fraction of the cold gas in previous inflows could have been rapidly accreted whilst forming few young stars. We note that an X_{CO} factor for BCGs that falls significantly below the Galactic value could alleviate several problems, including the demands on magnetic pressure and depletion of the hot gas. However, the low gas velocities in PKS 0745−191 and narrow velocity dispersions observed for molecular clouds in BCGs are inconsistent with the kinematic disturbances in starburst galaxies that require significantly lower X_{CO} factors. The low metal abundance suggests that the molecular gas mass could instead have been underestimated.

HST FUV observations of PKS 0745−191 show a bright spur of emission from young, massive star formation at 10-20 $\mathrm{M}_\odot$ yr^{-1} coincident with the SW molecular gas filament. The SW filament has a comparable velocity structure and mass to the other two filaments and such a clumpy, highly asymmetric distribution of gas about the nucleus does not appear consistent with a gas disc. The small-scale radio structure detected in 14.9 GHz VLA radio observations is also spatially coincident with the SW filament. A collision between an expanding radio structure and the molecular gas may have triggered collapse of the gas clouds and star formation in the SW filament. Disruption of the radio structure on small scales is also consistent with the amorphous radio morphology on larger scales in low-frequency observations. However, no increase in the velocity dispersion is observed either along the SW filament or by comparison with the other filaments.

ACKNOWLEDGEMENTS

HRR and ACF acknowledge support from ERC Advanced Grant Feedback 340442. BRM acknowledges support from the Natural Sciences and Engineering Council of Canada and the Canadian Space Agency Space Science Enhancement Program. PEJN was partly supported by NASA contract NAS8-03060. ACE acknowledges support from STFC grant ST/L00075X/1. GRT acknowledges support from Einstein Postdoctoral Fellowship Award Number PF-150128, issued by the Chandra X-ray Observatory Center, which is operated by the Smithsonian Astrophysical Observatory for and on behalf of NASA under contract NAS8-03060. We thank the reviewer for their thorough reading of the paper and encouraging comments. This paper makes use of the following ALMA data: ADS/JAO.ALMA 2012.1.00837.S. ALMA is a partnership of ESO (representing its member states), NSF (USA) and NINS (Japan), together with NRC (Canada), NSC and ASIAA (Taiwan), and KASI (Republic of Korea), in cooperation with the Republic of Chile. The Joint ALMA Observatory is operated by ESO, AUI/NRAO and NAOJ. The scientific results reported in this article are based on data obtained from the *Chandra* Data Archive. This publication makes use of data products from the 2MASS, which is a joint project of the University of Massachusetts and the Infrared Processing and Analysis Center/California Institute of Technology, funded by the National Aeronautics and Space Administration and the National Science Foundation.

REFERENCES

Alatalo K. et al., 2011, ApJ, 735, 88
Allen S. W., Fabian A. C., Kneib J. P., 1996, MNRAS, 279, 615

Arimoto N., Sofue Y., Tsujimoto T., 1996, PASJ, 48, 275
Baum S. A., O'Dea C. P., 1991, MNRAS, 250, 737
Best P. N., von der Linden A., Kauffmann G., Heckman T. M., Kaiser C. R., 2007, MNRAS, 379, 894
Bicknell G. V., Sutherland R. S., van Breugel W. J. M., Dopita M. A., Dey A., Miley G. K., 2000, ApJ, 540, 678
Bîrzan L., Rafferty D. A., McNamara B. R., Wise M. W., Nulsen P. E. J., 2004, ApJ, 607, 800
Bîrzan L., Rafferty D. A., Nulsen P. E. J., McNamara B. R., Röttgering H. J. A., Wise M. W., Mittal R., 2012, MNRAS, 427, 3468
Bolatto A. D., Leroy A. K., Rosolowsky E., Walter F., Blitz L., 2008, ApJ, 686, 948
Bolatto A. D., Wolfire M., Leroy A. K., 2013, ARA&A, 51, 207
Bower R. G., Benson A. J., Malbon R., Helly J. C., Frenk C. S., Baugh C. M., Cole S., Lacey C. G., 2006, MNRAS, 370, 645
Canning R. E. A. et al., 2014, MNRAS, 444, 336
Carilli C. L., Taylor G. B., 2002, ARA&A, 40, 319
Cavagnolo K. W., Donahue M., Voit G. M., Sun M., 2008, ApJ, 683, L107
Churazov E., Brüggen M., Kaiser C. R., Böhringer H., Forman W., 2001, ApJ, 554, 261
Crawford C. S., Sanders J. S., Fabian A. C., 2005, MNRAS, 361, 17
Croton D. J. et al., 2006, MNRAS, 365, 11
Daddi E. et al., 2010, ApJ, 714, L118
Dasyra K. M., Combes F., 2011, A&A, 533, L10
David L. P. et al., 2014, ApJ, 792, 94
Dey A., van Breugel W., Vacca W. D., Antonucci R., 1997, ApJ, 490, 698
di Serego Alighieri S. et al., 2007, A&A, 474, 851
Donahue M., Mack J., Voit G. M., Sparks W., Elston R., Maloney P. R., 2000, ApJ, 545, 670
Donahue M., de Messières G. E., O'Connell R. W., Voit G. M., Hoffer A., McNamara B. R., Nulsen P. E. J., 2011, ApJ, 732, 40
Downes D., Solomon P. M., 1998, ApJ, 507, 615
Draine B. T., Salpeter E. E., 1979, ApJ, 231, 77
Dunn R. J. H., Fabian A. C., 2006, MNRAS, 373, 959
Dunn R. J. H., Fabian A. C., 2008, MNRAS, 385, 757
Dwek E., Arendt R. G., 1992, ARA&A, 30, 11
Edge A. C., 2001, MNRAS, 328, 762
Egami E. et al., 2006, ApJ, 647, 922
Fabian A. C., 1994, ARA&A, 32, 277
Fabian A. C., 2012, ARA&A, 50, 455
Fabian A. C. et al., 1985, MNRAS, 216, 923
Fabian A. C., Johnstone R. M., Sanders J. S., Conselice C. J., Crawford C. S., Gallagher J. S., III, Zweibel E., 2008, Nature, 454, 968
Fabian A. C. et al., 2011, MNRAS, 418, 2154
Ferland G. J., Fabian A. C., Johnstone R. M., 1994, MNRAS, 266, 399
Ferland G. J., Fabian A. C., Hatch N. A., Johnstone R. M., Porter R. L., van Hoof P. A. M., Williams R. J. R., 2009, MNRAS, 392, 1475
Gaspari M., Brighenti F., Temi P., 2015, A&A, 579, A62
Govoni F., Feretti L., 2004, Int. J. Mod. Phys. D, 13, 1549
Graham J. A., Price R. M., 1981, ApJ, 247, 813
Grossi M. et al., 2009, A&A, 498, 407
Hamer S. L., Edge A. C., Swinbank A. M., Wilman R. J., Russell H. R., Fabian A. C., Sanders J. S., Salomé P., 2012, MNRAS, 421, 3409
Hatch N. A., Crawford C. S., Johnstone R. M., Fabian A. C., 2006, MNRAS, 367, 433
Heckman T. M., 1981, ApJ, 250, L59
Hernquist L., 1990, ApJ, 356, 359
Hicks A. K., Mushotzky R., 2005, ApJ, 635, L9
Hlavacek-Larrondo J., Fabian A. C., Edge A. C., Ebeling H., Sanders J. S., Hogan M. T., Taylor G. B., 2012, MNRAS, 421, 1360
Hogan M. T. et al., 2015, MNRAS, 453, 1201
Dinh-V-TrungHo I.-T., Lim J., 2009, ApJ, 698, 1191
Hu E. M., Cowie L. L., Wang Z., 1985, ApJS, 59, 447
Hunstead R. W., Murdoch H. S., Shobbrook R. R., 1978, MNRAS, 185, 149
Jaffe W., Bremer M. N., 1997, MNRAS, 284, L1
Jaffe W., Bremer M. N., Baker K., 2005, MNRAS, 360, 748
Johnstone R. M., Fabian A. C., Nulsen P. E. J., 1987, MNRAS, 224, 75
Kenney J. D. P., Young J. S., 1989, ApJ, 344, 171
Kennicutt R. C., Evans N. J., 2012, ARA&A, 50, 531
Kennicutt, R. C., Jr, 1998, ARA&A, 36, 189
Li Y., Bryan G. L., 2014, ApJ, 789, 153
Dinh-V-TrungLim J., Ao Y., 2008, ApJ, 672, 252
Ma C.-J., McNamara B. R., Nulsen P. E. J., Schaffer R., Vikhlinin A., 2011, ApJ, 740, 51
McKee C. F., Ostriker E. C., 2007, ARA&A, 45, 565
McMullin J. P., Waters B., Schiebel D., Young W., Golap K., 2007, in Shaw R. A., Hill F., Bell D. J., eds, ASP Conf. Ser., Vol. 376, Astronomical Data Analysis Software and Systems XVI. Astron. Soc. Pac., San Francisco, p. 127
McNamara B. R., Nulsen P. E. J., 2007, ARA&A, 45, 117
McNamara B. R., Nulsen P. E. J., 2012, New J. Phys., 14, 055023
McNamara B. R., O'Connell R. W., 1992, ApJ, 393, 579
McNamara B. R., Wise M., Sarazin C. L., Jannuzi B. T., Elston R., 1996, ApJ, 466, L9
McNamara B. R. et al., 2014, ApJ, 785, 44
Markwardt C. B., 2009, in Bohlender D. A., Durand D., Dowler P., eds, ASP Conference Series, Vol. 411, Astronomical Data Analysis Software and Systems XVIII. Astron. Soc. Pac., San Francisco, p. 251
Martin D. C. et al., 2007, Nature, 448, 780
Mittal R., Whelan J. T., Combes F., 2015, MNRAS, 450, 2564
Morganti R., Tadhunter C. N., Oosterloo T. A., 2005, A&A, 444, L9
Morganti R., Fogasy J., Paragi Z., Oosterloo T., Orienti M., 2013, Science, 341, 1082
Morganti R., Oosterloo T., Oonk J. B. R., Frieswijk W., Tadhunter C., 2015, A&A, 580, A1
Narayanan D., Krumholz M., Ostriker E. C., Hernquist L., 2011, MNRAS, 418, 664
Nesvadba N. P. H., Lehnert M. D., Eisenhauer F., Gilbert A., Tecza M., Abuter R., 2006, ApJ, 650, 693
O'Dea C. P. et al., 2008, ApJ, 681, 1035
Oonk J. B. R., Jaffe W., Bremer M. N., van Weeren R. J., 2010, MNRAS, 405, 898
Oosterloo T. A., Morganti R., 2005, A&A, 429, 469
Panagoulia E. K., Fabian A. C., Sanders J. S., 2013, MNRAS, 433, 3290
Peterson J. R., Fabian A. C., 2006, Phys. Rep., 427, 1
Pinkney J. et al., 1996, ApJ, 468, L13
Pizzolato F., Soker N., 2005, ApJ, 632, 821
Pizzolato F., Soker N., 2010, MNRAS, 408, 961
Quillen A. C. et al., 2008, ApJS, 176, 39
Rafferty D. A., McNamara B. R., Nulsen P. E. J., Wise M. W., 2006, ApJ, 652, 216
Rafferty D. A., McNamara B. R., Nulsen P. E. J., 2008, ApJ, 687, 899
Revaz Y., Combes F., Salomé P., 2008, A&A, 477, L33
Romanishin W., 1987, ApJ, 323, L113
Salomé P., Combes F., 2003, A&A, 412, 657
Salomé P. et al., 2006, A&A, 454, 437
Salomé P., Revaz Y., Combes F., Pety J., Downes D., Edge A. C., Fabian A. C., 2008, A&A, 483, 793
Salomé P., Combes F., Revaz Y., Downes D., Edge A. C., Fabian A. C., 2011, A&A, 531, A85
Salomé Q., Salomé P., Combes F., Hamer S., Heywood I., 2016, A&A, 586, A45
Sand D. J., Treu T., Ellis R. S., Smith G. P., 2005, ApJ, 627, 32
Sanders J. S., Fabian A. C., Hlavacek-Larrondo J., Russell H. R., Taylor G. B., Hofmann F., Tremblay G., Walker S. A., 2014, MNRAS, 444, 1497
Santoro F., Oonk J. B. R., Morganti R., Oosterloo T., 2015, A&A, 574, A89
Sharma P., Parrish I. J., Quataert E., 2010, ApJ, 720, 652
Shu F. H., 1992, The Physics of Astrophysics, Volume II: Gas Dynamics. University Science Books, Mill Valley, CA
Skrutskie M. F. et al., 2006, AJ, 131, 1163
Solomon P. M., Vanden Bout P. A., 2005, ARA&A, 43, 677
Solomon P. M., Rivolo A. R., Barrett J., Yahil A., 1987, ApJ, 319, 730
Solomon P. M., Downes D., Radford S. J. E., Barrett J. W., 1997, ApJ, 478, 144

Tadhunter C., Morganti R., Rose M., Oonk J. B. R., Oosterloo T., 2014, Nature, 511, 440
Taylor G. B., Sanders J. S., Fabian A. C., Allen S. W., 2006, MNRAS, 365, 705
Tremblay G. R. et al., 2015, MNRAS, 451, 3768
Ueda J. et al., 2014, ApJS, 214, 1
van Breugel W., Filippenko A. V., Heckman T., Miley G., 1985, ApJ, 293, 83
Voigt L. M., Fabian A. C., 2006, MNRAS, 368, 518
Voit G. M., Donahue M., 2011, ApJ, 738, L24
von der Linden A., Best P. N., Kauffmann G., White S. D. M., 2007, MNRAS, 379, 867
Wilman R. J., Edge A. C., Swinbank A. M., 2009, MNRAS, 395, 1355
Wilson C. D., 1995, ApJ, 448, L97
Young L. M. et al., 2011, MNRAS, 414, 940
Zubovas K., King A. R., 2014, MNRAS, 439, 400

This paper has been typeset from a TEX/LATEX file prepared by the author.